2D Basement Relief Inversion: A Comparative Study Among Multi-Objective Algorithms

Arthur A. C. R. Silva, Bruno M. Carvalho, Francisco M. Barboza
Federal University of Rio Grande do Norte - Brazil
arthur.romao@ufrn.br, bruno@dimap.ufrn.br, marcio.barboza@ufrn.br

***Abstract*—The gravimetric inversion of basement relief estimates the depth of density-contrast interfaces in the subsurface from measured gravitational anomalies. Such geophysical inverse problems are inherently ill-posed and unstable, requiring both regularization and efficient parameter estimation techniques. In this study, we apply and compare three multi-objective optimization algorithms — MOWGN, NSGA-II, and MOPSO — to minimize two conflicting objectives: (i) the misfit between observed and calculated gravity anomalies, and (ii) a smoothness regularization term (SM) to stabilize the inversion. The methods were implemented in MATLAB and tested on a real two-dimensional dataset from the Poem Bridge region. The comparison includes quantitative metrics — hypervolume, C-metric, and computational time — as well as qualitative assessments of Pareto front distribution, dominance, and smoothness of the estimated solutions. Statistical analyses were performed using the Mann–Whitney U test for pairwise comparisons and the Kruskal–Wallis test with Dunn–Bonferroni correction for multiple groups. The results reveal important differences in efficiency, robustness, and solution quality, providing practical insights into selecting the most suitable algorithm for real gravimetric inversion applications.**

***Keywords*—multi-objective optimization; gravimetry; regularization constraints; computational geophysics**

I. Introduction

The gravimetric method for estimating basement relief is a fundamental technique in geophysics, where computational algorithms play a central role. This method is particularly relevant for subsurface exploration, as it provides critical insights into geological structures and density contrasts that influence the observed gravity field [1]. However, accurately solving this inverse problem is challenging due to its ill-posed nature and sensitivity to data noise. The literature highlights the growing use of metaheuristics and advanced optimization algorithms to address these difficulties [2–7].

According to [8], geophysical inverse problems — including basement relief inversion — can be formulated as optimization problems in which the goal is to estimate model parameters, such as basement depths and density contrasts, within a feasible search space. The objective function quantifies the misfit between observed and modeled data, while additional constraints ensure physical plausibility. As noted by [9], these problems are typically ill-posed, characterized by non-uniqueness and instability in the presence of measurement noise. To mitigate these effects, a smoothness (SM) regularization constraint is introduced [10].

Multi-objective optimization provides a systematic framework for simultaneously minimizing multiple, often conflicting, objective functions. In this study, the inversion problem is formulated as a bi-objective task involving the minimization of the data misfit and a smoothness regularization term. The solution is represented by a Pareto front — a set of non-dominated solutions that balance the trade-off between fitting accuracy and model stability [11, 12].

Three algorithms were employed: the *Multi-Objective Weighted Gauss–Newton (MOWGN)*, the *Non-Dominated Sorting Genetic Algorithm II (NSGA-II)*, and the *Multi-Objective Particle Swarm Optimization (MOPSO)*. These algorithms were applied to the inversion of real gravimetric data from the Poem Bridge region, enabling a comparative evaluation of their performance and robustness in a realistic geophysical scenario [13–17].

The *MOWGN* algorithm is a local multi-objective method that combines gradient-based optimization with adaptive weighting through Lagrange multipliers. It generates a pseudo-random weight vector and uses a Jacobian-based iterative scheme to refine model parameters, producing an efficient local exploration of the Pareto front [18–21].

NSGA-II, proposed by [22], is a population-based evolutionary algorithm that ranks solutions using Pareto dominance. It employs crossover, mutation, and crowding-distance operators to ensure diversity and uniform coverage along the Pareto front, making it robust for non-linear and multimodal problems.

MOPSO, introduced by [23], extends the principles of particle swarm optimization to the multi-objective domain. It uses a repository of non-dominated solutions and a grid-based mechanism to maintain diversity while guiding particle movement through both individual and collective experiences, facilitating balanced exploration and exploitation.

The algorithms were compared using both quantitative and qualitative approaches. Quantitatively, performance was assessed using the hypervolume indicator, C-metric, and computational time. Qualitatively, Pareto fronts were analyzed to evaluate solution distribution, dominance, and smoothness of the reconstructed models. Statistical tests, including the Mann–Whitney U and Kruskal–Wallis with Dunn–Bonferroni correction, were used to verify the significance of differences among the algorithms [24–28].

The primary objective of this work is to develop and evaluate a robust methodology for estimating basement relief from real gravimetric data using multi-objective optimization. By integrating local and global optimization strategies within a regularized inversion framework, the study aims to enhance stability, reduce computational cost, and improve the quality of the reconstructed subsurface models. The findings contribute to advancing computational geophysics by providing reliable tools for resolving ill-posed inversion problems in complex geological environments.

II. Multi-Objective Optimization Framework

In the basement relief inversion problem, the goal is to estimate the basement depth distribution that best reproduces the observed gravity anomalies while maintaining geological plausibility. This involves balancing two competing objectives: minimizing the data misfit and enforcing smoothness through regularization.

The first objective function, $\Psi(\mathbf{d})$, measures the difference between observed and modeled gravity data, reflecting data fidelity. The second, $\Re(\mathbf{d})$, imposes smoothness to penalize abrupt variations, ensuring geologically consistent results. The decision vector $\mathbf{d} = (d_1, d_2, \ldots, d_N)$ represents the basement depths at discretized cells, constrained within physical bounds $\mathbf{d}_i^L$ and $\mathbf{d}_i^U$.

This bi-objective formulation, shown in Equation 1, defines an optimization problem in a two-dimensional objective space composed of misfit and regularization terms. The resulting Pareto frontier contains the non-dominated solutions representing optimal trade-offs between data fit and model smoothness.

$$\begin{aligned} &\min_{\mathbf{d}\in D} \ \mathbf{F}(\mathbf{d}) = [\Psi(\mathbf{d}),\ \Re(\mathbf{d})] \\ &\text{subject to:} \quad \mathbf{d}_i^L \leq \mathbf{d}_i \leq \mathbf{d}_i^U, \quad i = 1, 2, \ldots, N \end{aligned} \tag{1}$$

Here, the feasible region D represents admissible basement configurations. Each point on the Pareto frontier corresponds to a model that cannot improve one objective without degrading the other, thus reflecting a physically meaningful compromise between accuracy and stability.

A. Forward Model

The forward modeling process computes the theoretical gravity anomaly $\mathbf{g}(\mathbf{d})$ produced by a given basement geometry. The subsurface is represented as a set of 2D rectangular prisms, and the gravity anomaly at each observation point $P(x, z)$ is obtained by summing the contribution of all prisms:

$$g(d_i) = \sum_{j=1}^{n} f_j(\rho_j, d_j, r_{ij}), \quad i=1,2,\ldots,m;\ j=1,2,\ldots,n$$

$$\begin{aligned} f(\rho,d,r) = G\rho \Bigg[& A \ln\left(\frac{A^2+D^2}{A^2+C^2}\right) - B \ln\left(\frac{B^2+D^2}{B^2+C^2}\right) \\ & -2C\left(\arctan\left(\frac{A}{C}\right) - \arctan\left(\frac{B}{C}\right)\right) \\ & +2D\left(\arctan\left(\frac{A}{D}\right) - \arctan\left(\frac{B}{D}\right)\right) \Bigg] \end{aligned} \tag{2}$$

In this formulation, $r = (x, z)$ is the observation point, $d = (z_t, z_b)$ defines the top and bottom depths of each prism, and x_m, x_M denote its lateral limits. The auxiliary variables $A = r_x - x_m$, $B = r_x - x_M$, $C = r_z - z_t$, and $D = r_z - z_b$ simplify the computation of the gravitational effect. This analytical expression efficiently models sedimentary basins with variable basement topography.

B. Data Misfit Criterion

Following [29], the misfit functional Ψ quantifies the difference between observed and modeled gravity data:

$$\Psi(\mathbf{d}) = \frac{1}{m} \|\mathbf{g}^{obs} - \mathbf{g}(\mathbf{d})\|_2^2 \tag{3}$$

Here, $\mathbf{g}^{obs}$ is the observed gravity anomaly, and $\mathbf{g}(\mathbf{d})$ is the modeled response. The normalization factor $1/m$ scales the misfit by the number of observations. The function Ψ is nonlinear and continuously differentiable, suitable for gradient-based optimization.

C. Incorporating Regularization

Because the inversion problem is ill-posed, minimizing only the data misfit often yields unstable or oscillatory results. Regularization introduces stabilizing constraints that enforce desirable model properties [30, 31]. This converts the ill-posed problem into a stable one, producing geologically reasonable solutions.

1) Smoothness Regularization: Smoothness regularization penalizes rapid spatial variations in the model parameters [30]. Using a finite-difference approximation of the spatial gradient, the regularization term is expressed as:

$$\Re_{\text{smooth}}(\mathbf{d}) = \left\|\mathcal{D}\,\mathbf{d}\right\|_2^2, \tag{4}$$

where $\mathcal{D}$ is the finite-difference operator. This term suppresses abrupt depth changes, resulting in smoother and geologically plausible basement surfaces [32–34].

D. Optimization Methods

Three multi-objective optimization algorithms were used to solve the inversion problem: *MOWGN*, *NSGA-II*, and *MOPSO*. Each minimizes the data misfit and regularization terms but explores the search space differently, producing distinct Pareto fronts that represent trade-offs between data accuracy and smoothness.

1) MOWGN: The *MOWGN* method extends the Weighted Gauss–Newton algorithm to handle multiple objectives [18]. It uses the Jacobian matrix and second-order approximations for iterative minimization. Deterministic by nature, it offers fast local convergence but requires good initial estimates. It performs best when gradient information is reliable [8, 35, 36].

The algorithm starts with an initial model $\mathbf{d}_0$ estimated by the Bouguer plate approximation:

$$d_0^j = \frac{g_{obs}^j}{2\pi G\rho} \tag{5}$$

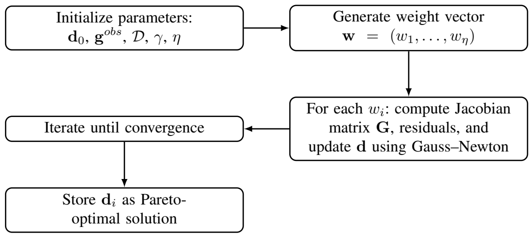

Figure 1. Workflow of the *MOWGN* algorithm.

A set of η weights $\mathbf{w}$ is used to balance data misfit and model smoothness. Each weight defines a scalarized objective function, which is solved iteratively until convergence. This process yields a set of Pareto-optimal solutions representing different trade-offs between accuracy and regularization. The workflow of the algorithm is illustrated in Fig. 1.

2) NSGA-II: The *NSGA-II* is an evolutionary algorithm that employs non-dominated sorting, elitism, and crowding distance to preserve diversity among candidate solutions [22, 37, 38]. As a population-based approach, it is particularly suitable for solving complex and multimodal optimization problems.

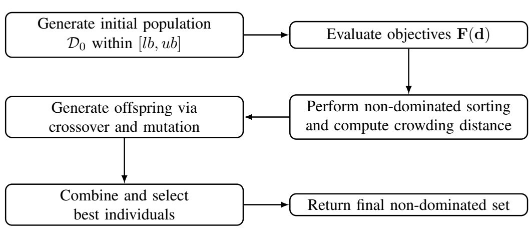

Figure 2. Workflow of the *NSGA-II*.

The initial population $\mathcal{D}_0$ is generated within bounds derived from the Bouguer estimate (Equation 5), defined as $lb = k_{\min} \cdot d_0$ and $ub = k_{\max} \cdot d_0$.

Following evaluation and ranking, *NSGA-II* iteratively refines the population through genetic operators, promoting both convergence and diversity. Over successive generations, this process leads to a well-distributed approximation of the Pareto front. The overall procedure is summarized in Fig. 2.

3) MOPSO: The *MOPSO* algorithm extends the classical PSO framework to handle multiple objectives. In this approach, particles update their positions and velocities based on personal and global best experiences, guided by leaders selected from a repository of non-dominated solutions. A grid-based mechanism is employed to preserve diversity [39–42].

MOPSO initializes particles within bounds derived from the Bouguer estimate (Equation 5), similarly to *NSGA-II*. Leaders are preferentially selected from less crowded regions of the search space to enhance exploration. Velocity updates incorporate inertia, cognitive, and social components with stochastic perturbations, while mutation operators help maintain diversity. The repository $\mathcal{R}$ is continuously updated throughout the iterations, leading to a well-distributed approximation of the Pareto front. The overall procedure is summarized in Fig. 3.

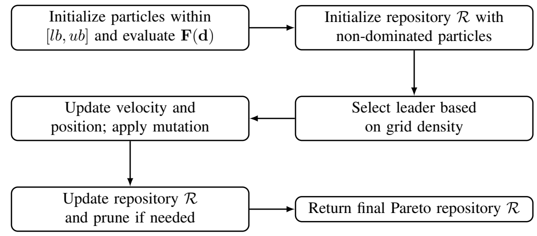

Figure 3. Workflow of the *MOPSO* algorithm.

III. Methodology

The experiments were performed using a real two-dimensional (2D) gravimetric dataset from the Poem Bridge region. In this case, model parameters were adjusted and optimized using three multi-objective evolutionary algorithms: *MOWGN*, *NSGA-II*, and *MOPSO*. All implementations and numerical analyses were carried out in MATLAB R2018b [43].

A. Poem Bridge

According to the studies by Lima [32] and Santos et al. [44], gravimetric inversion methodologies were applied to observed data from the Poem Bridge, located on the Belém Campus of the Federal University of Pará (UFPA). The left side of Figure 4 shows a photograph of the bridge's relief, highlighting the topographic gradients g_1 and g_2, as well as the reinforcement piles A and B, which act as sources of gravity anomalies due to their density contrast with the surrounding soil. The white lines represent topographic gradients across the profile; notably, the right-hand side of the image exhibits a smoother slope, while the left-hand side (west) shows a sharper discontinuity. The region beneath the bridge span, characterized by structural heterogeneity, defines the inversion domain.

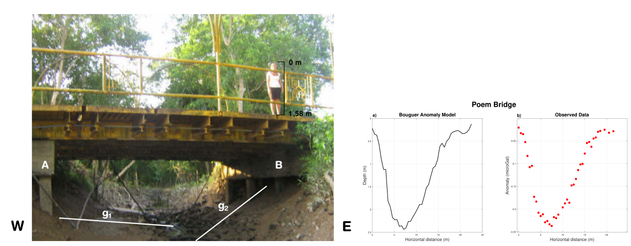

Figure 4. Left: Photograph including the W–E gravimetric profile of the Poem Bridge. The west side exhibits a more abrupt discontinuity than the east side. Source: [45]. Right: (a) Bouguer-based estimate of the subsurface structure beneath the Poem Bridge; (b) observed gravity profile.

The right side of Figure 4(a) presents the estimated model obtained from the Bouguer anomaly using the forward model described in Equation 5. In (b), the gravity anomalies correspond to the density contrast between air and soil, including the presence of reinforced concrete piles that generate localized anomalies.

In this interpretative model, a constant density contrast of $\rho = -2.3$ g/cm^3 was assumed. The analyzed profile spans a total length of 22.5 meters and was discretized into $n =$

45 rectangular prisms, each with a thickness of $\Delta v = 0.5$ m. A total of $m = 40$ gravity anomaly measurements were acquired along this profile. The maximum depth of the relief was estimated to be approximately 3.3 meters, based on the visual interpretation of the photograph presented in Figure 4, as described by Silva et al. [45].

Each algorithm was experimentally fine-tuned to ensure stable convergence and adequate exploration of the search space for the inversion of the Poem Bridge dataset. The initial model d_0 was derived from the Bouguer anomaly and used to define the search bounds, with $k_{\min} = 0.5$ and $k_{\max} = 1.5$, for both NSGA-II and MOPSO. In addition, both algorithms employed a population size $\eta = 500$ and a maximum number of iterations $\Gamma = 500$. *MOWGN* was configured with a maximum of 10 iterations, a Pareto front size $\Omega = 175$, and a weight vector $\mathbf{w}$ composed of random values drawn from the range $[0.1, 10]$. *NSGA-II* used a mutation rate $p_m = 0.01$, crossover rate $p_c = 0.75$, mutation factor $\kappa = 0.1$, and tournament size $\xi = 3$. Finally, *MOPSO* employed a repository size $\rho = 175$, grid divisions $\nu = 20$, acceleration coefficients $\phi_1 = 2$ and $\phi_2 = 2$, inertia weight $\omega = 1$, mutation rate $\mu = 0.1$, and maximum velocity $v_{\max} = 0.2 \cdot (ub - lb)$.

The Poem Bridge dataset provides a realistic and challenging scenario for evaluating the performance and robustness of multi-objective inversion algorithms. It includes near-surface targets, sharp topographic discontinuities, and heterogeneous subsurface structures—conditions commonly encountered in urban geophysical surveys. This real-case experiment enables a thorough and practical assessment of each algorithm's ability to balance convergence, diversity, and computational efficiency in complex gravimetric inversion problems.

IV. Results and Discussion

To evaluate the performance of the optimization algorithms, both quantitative and qualitative analyses were conducted using the real gravimetric dataset from the Poem Bridge region. In the quantitative analysis, two complementary evaluation perspectives were adopted: one focused on solution quality, based on the Hypervolume indicator, mean Euclidean distance to the Utopian point, and the C-metric; and another focused on computational efficiency, measured by the time required to generate the approximate Pareto-optimal solution sets. In the qualitative analysis, the Pareto fronts obtained from ten independent runs of each algorithm were merged, dominated solutions were removed, and representative points were selected for interpretation based on the reconstructed models and their corresponding data-fitting performance.

Hypothesis testing was performed with a significance level of $\alpha = 0.05$. Since the data did not follow a normal distribution and failed to meet the homogeneity of variance assumption, non-parametric statistical tests were used. For pairwise comparisons involving the binary C-metric, the Mann–Whitney U test was applied. For the unary indicators (Hypervolume, Euclidean Distance, and Computational Time), the Kruskal–Wallis test followed by Dunn–Bonferroni post hoc correction was used.

A. Quantitative Analysis

Hypervolume: The Hypervolume indicator evaluates the distribution and spread of solutions along each algorithm's Pareto front with respect to a fixed reference point. The null hypothesis (H_0) stated that "there is no significant difference in the hypervolume values among the ten approximate solution sets generated by each algorithm." The observed p-value (0.0006) led to the rejection of H_0 in favor of the alternative hypothesis (H_1), indicating significant differences among the algorithms. According to the Dunn–Bonferroni post-hoc test, statistically significant differences were observed between *MOWGN* and *NSGA-II* ($p = 0.0010$), and between *NSGA-II* and *MOPSO* ($p = 0.0069$).

Figure 5 illustrates these results by combining the Pareto fronts obtained from the three algorithms. Each front was generated after ten independent runs, and all non-dominated solutions were merged while removing dominated points to form the composite Pareto fronts.

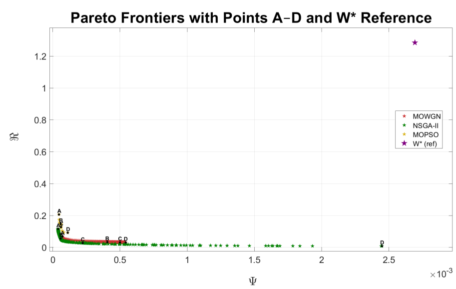

Figure 5. Pareto fronts of the *MOWGN*, *NSGA-II*, and *MOPSO* algorithms with representative points, along with the reference point.

Based on the median hypervolume values, the ranking is as follows: *MOWGN* (0.0027), *MOPSO* (0.0026), and *NSGA-II* (0.0010). These results indicate that *MOWGN* and *MOPSO* produced more extensive and better-distributed Pareto fronts than *NSGA-II*, suggesting superior exploration capabilities of the objective space.

C-Metric: The C-metric evaluates dominance relationships among the Pareto fronts of different algorithms. An algorithm that dominates a larger portion of another algorithm's front is considered superior, though cases of incomparability may occur [24]. Since the C-metric is binary, pairwise comparisons were conducted. The null hypothesis (H_0) assumed no significant dominance difference between the solution sets of algorithms A and B. The results were as follows:

- *MOWGN* vs *NSGA-II*: Median(*MOWGN* $\rightarrow$ *NSGA-II*) = 0.0000; Median(*NSGA-II* $\rightarrow$ *MOWGN*) = 1.0000; $p = 0.0000 \Rightarrow$ *NSGA-II* significantly dominates *MOWGN*.
- *MOWGN* vs *MOPSO*: Median(*MOWGN* $\rightarrow$ *MOPSO*) = 0.2679; Median(*MOPSO* $\rightarrow$ *MOWGN*) = 0.0000; $p = 0.0002 \Rightarrow$ *MOWGN* significantly dominates *MOPSO*.
- *NSGA-II* vs *MOPSO*: Median(*NSGA-II* $\rightarrow$ *MOPSO*) = 0.7571; Median(*MOPSO* $\rightarrow$ *NSGA-II*) = 0.0000; $p = 0.0001 \Rightarrow$ *NSGA-II* significantly dominates *MOPSO*.

Based on the number of dominance wins, the overall ranking is: *NSGA-II* (dominates both *MOWGN* and *MOPSO*), followed by *MOWGN*, and then *MOPSO*. These findings reinforce the robustness of *NSGA-II* in maintaining high-quality non-dominated solutions across different regions of the Pareto front.

Computational Efficiency: This metric quantifies the total computational time required to produce the approximate Pareto fronts. The null hypothesis (H_0) stated that "There are no significant differences in computational time among the algorithms." The test yielded a p-value of 0.0000, indicating statistically significant differences. According to the Dunn–Bonferroni correction, significant differences were observed between *MOWGN* and *NSGA-II* ($p = 0.0333$), *MOWGN* and *MOPSO* ($p = 0.0000$), and *NSGA-II* and *MOPSO* ($p = 0.0333$). Thus, the ranking based on median computational time is: **1st** - *MOWGN* (9.2367 s), **2nd** - *NSGA-II* (52.8286 s) and **3rd** - *MOPSO* (147.1504 s).

MOWGN was substantially faster, confirming its computational advantage due to its deterministic nature and the use of gradient-based search. *NSGA-II* presented intermediate performance, balancing solution quality and efficiency, whereas *MOPSO* required considerably longer execution times due to the iterative particle updates and global-best communication steps inherent to swarm-based algorithms.

B. Qualitative Analysis

To visually support the quantitative findings, the solution sets of each algorithm were merged, dominated solutions were removed, and four representative points (A, B, C, and D) were selected along each Pareto front, as shown in Fig. 5. These points were used to compare the observed and calculated Bouguer anomaly data. Reconstructed geological models are presented in Fig. 6.

The *MOWGN* algorithm exhibited excellent convergence, but with a limited spread of solutions near the region emphasizing data misfit minimization. The reconstructed models obtained from the selected Pareto points demonstrated consistent convergence toward the expected subsurface structure of the Poem Bridge Basin, producing smooth interfaces and stable density contrasts.

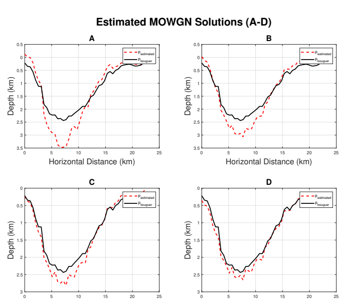

Figure 6. Points A, B, C, and D of the Pareto front from the *MOWGN* algorithm in the 2D inversion of the Poem Bridge Basin, with the Bouguer anomaly model and estimated solutions.

The *NSGA-II* algorithm presented a Pareto front characterized by good convergence and smooth distribution of solutions. Despite minor unevenness in the region dominated by regularization, the algorithm achieved high-quality trade-offs between the two objectives. The inversion results obtained with *NSGA-II* were geologically plausible and consistent with prior works on the Poem Bridge Basin [32, 44], showing well-defined basement structures and realistic sedimentary thickness variations.

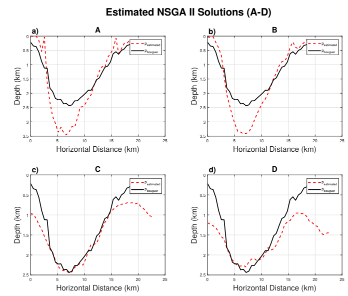

Figure 7. Points A, B, C, and D of the Pareto front from the *NSGA-II* algorithm in the 2D inversion of the Poem Bridge Basin, with the Bouguer anomaly model and estimated solutions.

The *MOPSO* algorithm achieved reasonable convergence toward the Pareto front but displayed less uniform distribution of solutions. This uneven spacing slightly limited the exploration of intermediate trade-off regions between the two objectives. Nevertheless, the resulting models were geologically coherent, reproducing the main structural trends of the basin and maintaining good agreement between the observed and calculated anomalies.

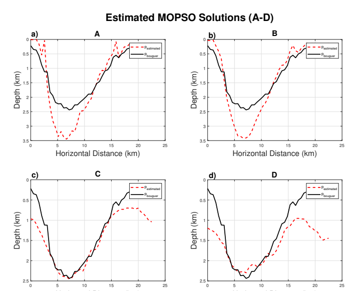

Figure 8. Points A, B, C, and D of the Pareto front from the *MOPSO* algorithm in the 2D inversion of the Poem Bridge Basin, with the Bouguer anomaly model and estimated solutions.

The *MOPSO* results indicate that, despite limited solution diversity, the algorithm produced geologically consistent interpretations of the Poem Bridge Basin structure. Overall, the qualitative analyses confirmed the quantitative findings: *MOWGN* achieved superior computational efficiency, *NSGA-II* provided the best balance between convergence and solution diversity, and *MOPSO*, while computationally more demanding, still delivered geologically valid results with stable inversion behavior.

V. Conclusion

This study evaluated the performance of three multi-objective optimization algorithms — *MOWGN*, *NSGA-II*, and

MOPSO — applied to the gravimetric inversion of real data from the Poem Bridge region. The inversion was formulated as a bi-objective problem, balancing data misfit and first-order Tikhonov regularization. Performance assessment considered both quantitative indicators (Hypervolume, Euclidean Distance to the Utopian Point, C-Metric, and Computational Time) and qualitative analysis of the recovered geological structures.

In the real-data case analyzed, *MOWGN* demonstrated superior computational efficiency, achieving faster convergence and satisfactory Pareto front coverage. *NSGA-II* provided the most balanced trade-off between convergence and diversity, dominating the solution space according to the C-metric and producing a broader distribution of plausible models. Although *MOPSO* exhibited lower diversity, it was still capable of generating geologically consistent and stable solutions.

Overall, the results indicate that *MOWGN* is preferable when computational cost is a primary concern, while *NSGA-II* offers greater robustness and exploration capability for complex real-world inversions. *MOPSO* remains a viable alternative when moderate accuracy and simpler parameterization are acceptable. Future work may focus on developing a hybrid approach that combines the strengths of *MOWGN* and *NSGA-II* to achieve both efficient convergence and enhanced solution diversity.

ACKNOWLEDGEMENTS

This study was financed in part by the Coordenação de Aperfeiçoamento de Pessoal de Nível Superior - Brasil (CAPES) - Finance Code 001.

REFERENCES

[1] W. M. Telford, L. P. Geldart, and R. E. Sheriff, *Applied Geophysics*. Cambridge Univ. Press, 1990.

[2] M. A. Al-Garni, "Inversion of residual gravity anomalies using neural network," *Arabian J. Geosci.*, vol. 6, pp. 1509–1516, 2013.

[3] J. Pallero *et al.*, "Gravity inversion and uncertainty assessment of basement relief via particle swarm optimization," *J. Appl. Geophys.*, vol. 116, pp. 180–191, 2015.

[4] A. Joolaei *et al.*, "Basement relief modeling by gravity inversion via ant colony algorithm," *Iran. J. of Geophys.*, vol. 14, no. 1, pp. 39–54, 2020.

[5] S. He *et al.*, "Recovering 3D basement relief using gravity data through convolutional neural networks," *J. Geophys. Res.: Solid Earth*, vol. 126, no. 10, p. e2021JB022611, 2021.

[6] Q. Yang *et al.*, "3-D gravity inversion based on deep convolution neural networks," *IEEE Geosci. Remote Sens. Lett.*, vol. 19, pp. 1–5, 2021.

[7] C. Dubey *et al.*, "Basement relief of sedimentary basin using gravity data from deep neural network approach," *J Geol Geophys*, vol. 12, p. 1066, 2023.

[8] M. K. Sen and P. L. Stoffa, *Global Optimization Methods in Geophysical Inversion*. Cambridge Univ. Press, 2013.

[9] J. Hadamard, "Sur les problèmes aux dérivées partielles et leur signification physique," 1902, Princeton Univ. Bull., pages 49–52.

[10] A. N. Tikhonov, "On the solution of incorrectly stated problems and a method of regularization," in *Dokl. Acad. Nauk. SSSR*, vol. 151, 1963, pp. 501–504.

[11] J. L. Cohon, *Multiobjective Programming and Planning*. Courier Corp., 2013.

[12] K. Deb, *Multiobjective Optimization Using Evolutionary Algorithms*. New York: Wiley, 2001.

[13] J. Xiong and T. Zhang, "Multiobjective particle swarm inversion algorithm for two-dimensional magnetic data," *Appl. Geophys.*, vol. 12, no. 2, pp. 127–136, 2015.

[14] S. Schnaidt *et al.*, "Pareto-optimal multi-objective inversion of geophysical data," *Pure Appl. Geophys.*, vol. 175, no. 6, pp. 2221–2236, 2018.

[15] F. Pace *et al.*, "Joint optimization of geophysical data using multi-objective swarm intelligence," *Geophys. J. Int.*, vol. 218, no. 3, pp. 1502–1521, 2019.

[16] F. M. Barboza, A. A. d. C. R. E. Silva, and B. M. Carvalho, "2D basement relief inversion using sparse regularization," https://arxiv.org/abs/2410.14942, 2024, arXiv.

[17] R. Sharma *et al.*, "Joint inversion of DC resistivity and MT data using multi-objective grey wolf optimization," in *NSG 2024 30th Eur. Meet. of Environm. and Engin. Geophys.*, vol. 2024, 2024, pp. 1–5.

[18] M. A. Meju, *Geophysical Data Analysis: Understanding Inverse Problem Theory and Practice*. Soc. Explor. Geophys., 1994.

[19] W. Murray, M. H. Wright, and P. E. Gill, *Practical Optimization*. SIAM-Soc. Ind. and Appl. Math., 2019.

[20] P. C. Hansen, "The L-curve and its use in the numerical treatment of inverse problems," IMM, Tech. Univ. of Denmark, Tech. Rep. IMM-REP-1999-15, 1999.

[21] D. P. Bertsekas, *Constrained Optimization and Lagrange Multiplier Methods*. Acad. Press, 2014.

[22] K. Deb *et al.*, "A fast and elitist multiobjective genetic algorithm: NSGA-II," *IEEE Trans. Evol. Comput.*, vol. 6, no. 2, pp. 182–197, 2002.

[23] C. C. Coello and M. S. Lechuga, "MOPSO: A proposal for multiple objective particle swarm optimization," in *Proc. of CEC*, vol. 2. IEEE, 2002, pp. 1051–1056.

[24] E. Zitzler, "Evolutionary algorithms for multiobjective optimization," in *Evolutionary Methods for Design, Optimization and Control*, K. Giannakoglou *et al.*, Eds. Barcelona, Spain: CIMNE, 1998.

[25] ——, *Evolutionary Algorithms for Multiobjective Optimization: Methods and Applications*. Shaker Ithaca, 1999, vol. 63.

[26] W. H. Kruskal and W. A. Wallis, "Use of ranks in one-criterion variance analysis," *J. Am. Stat. Assoc.*, vol. 47, no. 260, pp. 583–621, 1952.

[27] O. J. Dunn, "Multiple comparisons using rank sums," *Technom.*, vol. 6, no. 3, pp. 241–252, 1964.

[28] M. Hollander *et al.*, *Nonparametric Statistical Methods*. John Wiley & Sons, 2013.

[29] J. B. Silva *et al.*, "Pitfalls in nonlinear inversion," *Pure Appl. Geophys.*, vol. 158, no. 5-6, pp. 945–964, 2001.

[30] A. N. Tikhonov and V. Y. Arsenin, *Solutions of Ill-posed Problems*. New York: John Wiley & Sons, 1977, vol. 1.

[31] H. W. Engl *et al.*, *Regularization of Inverse Problems*. Springer Sci. & Bus. Media, 1996, vol. 375.

[32] W. A. Lima, "Inversão gravimétrica do relevo de bacias extencionais através da variação total," Master's thesis, PPgG, UFPA, 2009.

[33] J. B. Silva *et al.*, "Gravity inversion of 2D basement relief using entropic regularization," *Geophys.*, vol. 75, no. 3, pp. I29–I35, 2010.

[34] F. M. Barboza *et al.*, "A user-driven feedback approach for 2D direct current resistivity inversion based on particle swarm optimization," *Geophys.*, vol. 84, no. 2, pp. E105–E124, 2019.

[35] A. Tarantola, *Inverse Problem Theory and Methods for Model Parameter Estimation*. SIAM, 2005.

[36] P. G. Lelievre, R. Bijani, and C. G. Farquharson, "Joint inversion using multi-objective global optimization methods," in *78th EAGE Conf. and Exhib.* Europ. Assoc. Geoscientists & Engineers, 2016, pp. 1–5.

[37] C. C. Coello, "Evolutionary multi-objective optimization: A historical view of the field," *IEEE Comp. Intel. Mag.*, vol. 1, pp. 28–36, 2006.

[38] A. Zhou *et al.*, "A multiobjective evolutionary algorithm based on decomposition and probability model," in *CEC*. IEEE, 2012, pp. 1–8.

[39] C. A. Coello *et al.*, "Handling multiple objectives with particle swarm optimization," *IEEE Trans. Evol. Comput.*, vol. 8, pp. 256–279, 2004.

[40] S. Mostaghim and J. Teich, "Strategies for finding good local guides in multi-objective particle swarm optimization (MOPSO)," in *Proc. IEEE Swarm Intell. Symp.*, 2003, pp. 26–33.

[41] R. Eberhart and J. Kennedy, "A new optimizer using particle swarm theory," in *MHS*. IEEE, 1995, pp. 39–43.

[42] J. J. Durillo and A. J. Nebro, "jMetal: A Java framework for multi-objective optimization," *Adv. Engin. Software*, vol. 42, no. 10, pp. 760–771, 2011.

[43] The MathWorks, Inc., *MATLAB R2018b*, The MathWorks, Inc., Natick, MA, USA, 2018, version 9.5 (R2018b). [Online]. Available: https://www.mathworks.com/products/matlab.html

[44] R. D. C. S. d. Santos *et al.*, "Inversão gravimétrica rápida do relevo do embasamento aplicando o funcional da variação total," Master's thesis, UFPA, Brazil, 2013.

[45] J. B. C. Silva *et al.*, "Inversão gravimétrica do relevo do embasamento usando regularização entrópica," in *10th Int. Cong. Brazil. Geophys. Soc. & EXPOGEF 2007, Rio de Janeiro, Brazil*, 2007, pp. 698–703.